

# CAPTURING GEOLOGICAL REALISM IN STOCHASTIC SIMULATIONS OF ROCK SYSTEMS WITH MARKOV STATISTICS AND SIMULATED ANNEALING

KEVIN P. PARKS<sup>1</sup>, LAURENCE R. BENTLEY<sup>2</sup>, AND ALLAN S. CROWE<sup>3</sup>

<sup>1</sup> Alberta Geological Survey, Alberta Energy and Utilities Board, 4th Floor, 4999-98th Avenue, Edmonton, Alberta T6B 2X3, Canada  
email: kpark@petro-canada.ca

<sup>2</sup> Department of Geology and Geophysics, University of Calgary, 2500 University Drive, Calgary, Alberta T2N 1N4, Canada

<sup>3</sup> National Water Research Institute, Canada Centre for Inland Waters, P.O. Box 5050, Burlington, Ontario L7R 4A6, Canada

**ABSTRACT:** Simulated annealing is a numerical algorithm that can be used to impose statistical structures on numerical grids representing heterogeneous rock or sediment. In this paper, we use the flexibility of simulated annealing to generate grids with Markov statistical structures. Our purpose is to transmit the rich geological information captured in Markov statistics into stochastic grids while maintaining the flexibility of annealing to honor field data. Performance issues that compromise annealing grids imbued with Markovian properties include scales of bedding or rock bodies relative to grid size, and the amount of geological complexity in the embedded Markov structures. The remedies to these issues include proper selection of grid size, careful choice of annealing type, and consideration of an alternative annealing stopping rule based on a chi-squared test statistic. If performance issues are overcome, complex stratal patterns such as higher-order dependency, cyclicity, and directionality can be replicated in grids by this method. In addition, accounting for variations in depositional rate allows for transference of Markov structures obtained from vertical boreholes to the horizontal dimension when other information is lacking. A field example using borehole data collected at the Gloucester special waste site near Ottawa, Canada, as well as synthetic examples, demonstrate the technique and performance issues.

## INTRODUCTION

Simulation of multiple, equiprobable heterogeneous grids (so-called stochastic simulations) for flow simulators and the like can be done by a variety of methods (Koltermann and Gorelick 1996). A practical challenge to their implementation remains how to better constrain simulations to match geological concepts of reasonableness (Deutsch and Hewitt 1996). Doveton (1994) suggested that Markov models could play a role in transmitting realism into geological simulations. In this paper we document the performance issues related to the construction of two-dimensional stochastic fields with Markov properties using simulated annealing and the multipoint histogram method of Deutsch and Journel (1992). We demonstrate how meaningful stratal geometry can be effectively reproduced in stochastic fields by imbuing them with a Markov structure. Synthetic examples demonstrate the results alongside a field trial using core data. The core data come from heterogeneous glacial sediments at the Gloucester special waste site, Ontario (Fig. 1).

Various methods exist to directly generate Markov fields (Krumbein 1967; Harbaugh and Bonham-Carter 1970; Lin and Harbaugh 1984; Moss 1990; Luo 1996) or use Markov structures to improve, inform, or calibrate other geostatistical simulation methods (e.g., Murray 1994; Carle and Fogg 1996). But despite their obvious attraction to geologists and long association with description and simulation of one-dimensional bedding sequences (e.g., Walker 1979, Chen 1999), direct simulation of Markov fields has had relatively little penetration into the practice of stochastic simulation. Koltermann and Gorelick (1996) cite the difficulty of conditioning pure Markov fields to other types of field data as a barrier to their practical use. Simulated annealing, a flexible numerical algorithm used to generate stochastic fields conditioned to different types of field data, has qualities that

may allow improved integration of Markov descriptors in stochastic grids conditioned to honor field data.

The main purpose of this paper is to document the performance characteristics of using simulated annealing to create Markov fields with and without conditioning. We offer remedies to some of the implementation problems so as to expand the use of both Markov statistics and simulated annealing in stochastic simulation.

## CONSTRUCTING MARKOV FIELDS WITH SIMULATED ANNEALING

### *Markov Chains and Fields in Geological Applications*

A discrete sequence of events wherein the present state or category of the sequence is contingent on the state of the sequence at some time prior is said to be a Markov chain. Two- and three-dimensional spatial fields can also have Markov properties (Lin and Harbaugh 1984). The following paragraphs offer a brief overview of Markov statistics. Doveton (1994), Davis (1986), and Schwarzacher (1975) provide complete introductions to the use of Markov statistics in geology.

In their common form, Markov statistics are presented in the form of a transition probability matrix (e.g., Table 1). The matrix tabulates the conditional probability that a time or space series stays in the same category or enters a different category with each succeeding step given the category the chain occupies at present. The matrix is usually derived by counting observations of category (like lithology) at equally spaced increments along a transect. The transition frequencies are tabulated by category in a matrix (e.g., Table 1A). The frequencies are then normalized by their row totals to determine the conditional probabilities (e.g., Table 1B). A chi-squared statistical test is usually applied to an experimental Markov matrix to determine if the transitions collectively or individually are significantly different than a random series of events. Powers and Easterling (1982) provide a comprehensive discussion on statistical testing of Markov matrices in geological applications.

A Markov chain developed over a single step or unit lag,  $n = 1$ , is called first order. Markov chains developed from observations at two different lags are termed second order. Because Markov statistics are conditional probabilities, conditional probabilities for lags  $n > 1$  can be determined by powering the Markov matrix to the  $n$ th exponent through successive matrix multiplications or matrix factorization methods (Schwarzacher 1975). The expected proportions of each category can be obtained by powering the matrix until the column vectors stabilize (Davis 1986), at which time they represent independent or unconditional probabilities of occurrence (e.g., Table 1D). The thickness or duration of each category in a first-order Markov process is geometrically distributed with an arithmetic mean,  $m_{ii}$ , approximated by

$$m_{ii} = \frac{p_{ii}}{1 - p_{ii}} \Delta \quad (1)$$

where  $p_{ii}$  is the value of the diagonal element in the  $i$ th row of the transition probability matrix and  $\Delta$  is the step length in the chain (Doveton 1994).

The size of the sampling interval in a Markov-chain analysis must be chosen carefully (Schwarzacher 1975). In bedded sequences, too small an

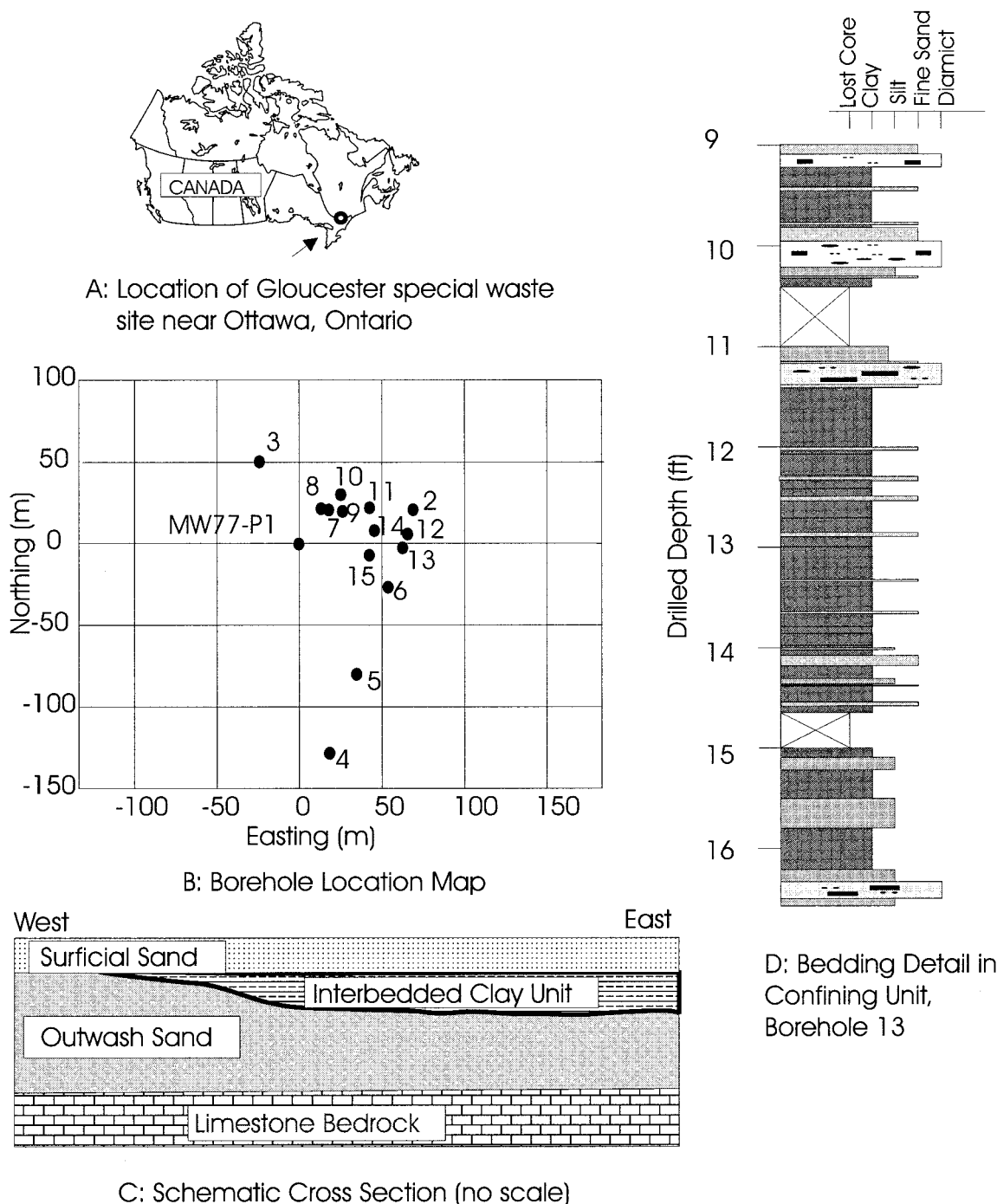


FIG. 1.—A) Location of Gloucester special waste site near Ottawa, Ontario, Canada. B) Borehole map of Gloucester special waste site boreholes for this study with monitoring well MW77-P1 (Jackson et al. 1991) for reference. C) Schematic cross section illustrating site Quaternary lithostratigraphy. D) Representative lithology log showing bedding heterogeneity in clay unit from Borehole 13.

increment results in a diagonally dominant Markov matrix. A diagonally dominant matrix is a matrix with large values in the diagonal elements and small values in off-diagonal elements. Choice of too large an increment causes thin interbeds and rare events to be missed. To compensate for sample-size effects, geologists collecting Markov statistics also use a derived form of the matrix called the embedded form (e.g., Table 1C). In the embedded form, only the transitions between different categories are encapsulated in the transition probability matrix—the step size is not a unit

of length measure but the beds themselves. The embedded form can be calculated from a Markov chain simply by setting the diagonal values in a regular Markov matrix to zero and renormalizing the off-diagonal elements by their new sum. Embedded Markov structures have been used to identify nonrandom facies associations in bedding sequences (e.g., Walker 1979; Xu and MacCarthy 1996).

One of the other attractions of Markov statistics is that they can capture asymmetries in the between-category relationships, allowing for capture of

TABLE 1.—A) A first-order, five-state Markov transition-frequency matrix for the clay unit at the Gloucester site. B) The resulting transition-probability matrix and C) its embedded form. D) The stabilized column vectors obtained after powering the matrix in C) one hundred times.

P(J) I	Med. Sand	Fine Sand	Silt	Clay	Diamict
Med. Sand	78	4	3	1	1
Fine Sand	2	339	11	46	8
Silt	4	8	110	14	7
Clay	1	44	20	680	10
Diamict	4	10	0	8	136
A) Lithofacies transition-frequency matrix					
Med. Sand	0.8965	0.0460	0.0345	0.0115	0.0115
Fine Sand	0.0049	0.8350	0.0271	0.1133	0.0197
Silt	0.0290	0.0580	0.7971	0.1014	0.0145
Clay	0.0013	0.0583	0.0265	0.9007	0.0132
Diamict	0.0253	0.0633	0.0000	0.0506	0.8608
B) Transition probability matrix					
Med. Sand	0.0000	0.4444	0.3333	0.1111	0.1111
Fine Sand	0.0297	0.0000	0.1642	0.6867	0.1194
Silt	0.1429	0.2859	0.0000	0.4998	0.0715
Clay	0.0131	0.5871	0.2669	0.0000	0.1329
Diamict	0.1818	0.4547	0.0000	0.3635	0.0000
C) Embedded transition-probability matrix.					
Med. Sand	0.0723	0.2590	0.1070	0.4634	0.0979
Fine Sand	0.0723	0.2590	0.1070	0.4634	0.0979
Silt	0.0723	0.2590	0.1070	0.4634	0.0979
Clay	0.0723	0.2590	0.1070	0.4634	0.0979
Diamict	0.0723	0.2590	0.1070	0.4634	0.0979
D) Independent transition probabilities or expected proportions of each state.					

preferred directionality, complex associations, and cyclicity in geologic structures that are the signal of a depositional process and time's arrow (Carle and Fogg 1996). Asymmetrical Markov transition matrices can also generate structured random fields with multifractal characteristics (Chen 1999).

#### Going from the Vertical to the Horizontal with Walther's Law

A recurrent problem in the implementation of any stochastic modeling technique is how to gather or infer horizontal relationships from widely spaced or sparse vertical boreholes. Data structures from horizontal wells, depositional process simulators, outcrops, or densely drilled analogous sites are among the available alternatives for informing horizontal relationships. Doveton (1994) revisits the common notion that Markov measures of vertical variability from boreholes can be transferred directly to the horizontal to inform a description of horizontal variability in circumstances of data scarcity. The geological justification for this transference comes through invocation of Walther's Law of Facies Succession, an operating principle of stratigraphy (see Middleton 1973 for a review). Recast in Markovian terms, one might restate Walther's Law as follows: if the probability of any state succeeding another in the vertical is equal to the probability that the states developed adjacently at a given time, then the probabilities of any state being juxtaposed horizontally should equal the probability that states are vertically superimposed, provided that the horizontal juxtaposition is coeval. The probabilistic approach can also accommodate minor erosional breaks in a succession as a component of random noise so long as the depositional process remains stationary at the scale of interest (Doveton 1994).

#### Markovian Descriptions of Complex Heterogeneity at The Gloucester Special Waste Site, Ontario

To examine the performance issues related to generating stochastic representations of complex subsurface rock bodies by Markov statistics using simulated annealing, a variety of synthetic Markov structures are used in

this study. These are discussed further below. As a simultaneous test of practical implementation, a real Markov data set of a complex Quaternary deposit is also used. Simulations of this deposit act as a test of whether this approach to incorporating geological information offers tangible rewards for a reasonable effort from the point of view of the practicing geologist involved in simulation.

The five-state, first-order Markov chain derived from real field data is shown in Table 1. The lithologic data in the transition frequency matrix come from vertical cores taken from fifteen 5 m boreholes through a thinly interbedded sedimentary sequence at the Gloucester special waste site near Ottawa, Canada (Fig. 1).

The Ottawa region is blanketed by glacial sediments of Late Wisconsin age. Most of these Quaternary sediments are tills, but glaciofluvial, glaciolacustrine, and glaciomarine sediments are also abundant. Overlying much of the glacial sediments are deposits of the Champlain Sea, a marine incursion that followed Wisconsin deglaciation. Eskers and subaqueous delta-fan complexes are common. These features mark the drainage patterns and outflows of subglacial meltwater conduits (Fulton et al. 1987).

The unconsolidated Quaternary sediments underlying our drilling site define three lithostratigraphic units: a fine quartz sand about 2 m thick; a 3-m-thick silty clay unit with thin interbeds of diamict, silt, fine quartz sand, and stiff clay; and a medium- to coarse-grained quartz sand about 20 m thick overlying limestone bedrock. A conceptual cross section and representative strip log through the clay unit are also shown in Figure 1. In this study we look at the 3 m clay unit, not the entire sequence.

The sediments of the interbedded clay layer and the underlying sand are interpreted to be deposits of coalescent, subaqueous deltas that built out from subglacial drainage tunnels into meltwater lakes in front of retreating glaciers. The clay unit represents the distal bottomset aprons coeval with the proximal sandy topset and foreset beds (Jackson et al. 1991). Rust (1977) reasoned that much of the heterogeneity in these outwash deposits is due to a combination of deposition in distributary channels on the outwash fans and mass wasting processes on their flanks. Our drilling site was selected on the basis of the presence of these fluviodeltaic deposits, which tend to have nonrandom facies associations amenable to Markov analysis (e.g., Miall 1980), plus the fact that these deposits lie very close to the surface at the Gloucester special waste site.

The Markov statistics in Table 1 were derived by logging the internal lithology of core from the clay unit. A layer-thickness cutoff of 2 mm for recording was used, meaning that much of the logging was done under a microscope. We found that such a small cutoff was necessary to capture rare transitions in the unit. The results from all the boreholes were combined under the assumptions that the process of formation was homogeneous across the drill site and that the boreholes were far enough from each other to represent independent samples of the process of deposition. The number of transitions from any state to itself or different states along an 8 mm spacing were then counted to form the transition frequency matrix (Table 1A). Because of the small sample spacing, the transition frequency matrix and the transition probability matrix (Table 1B) are diagonally dominant. The embedded structure was also determined (Table 1C).

A chi-squared test on the entire transition matrix determined that the Markov matrix as a whole was significantly different than a random series of events. This is actually a trivial result virtually guaranteed in a diagonally dominant transition probability matrix. The data were also examined for second-order structure. No significant second-order structure could be detected up to a secondary lag of 30 mm. The embedded Markov structure (Table 1C) was tested with a modified chi-squared test (Davis 1986) and found to be no different than a random series of events. This lack of structure is consistent with the interpretation that the sedimentary process was dominated by episodic events linked to ice wasting.

#### Simulated Annealing

Simulated annealing is a global optimization method whereby a grid or field that honors an idealized set of control statistics can be generated in a

stochastic framework. Gateway references to the details of annealing methodology are Ouenes and Bhagavan (1994) and Jensen et al. (1997). The essence of the annealing methodology is summarized below.

To generate a stochastic field or image by annealing, an idealized or training field is first characterized by a combination of statistical or other descriptive measurements, e.g.,  $I = f(a_I, b_I, c_I, \dots)$ . These descriptors can be derived from theoretical study or field measurements. A trial field is then generated. The trial field can be a totally random image matching the ideal global histogram or a structured field created by a different algorithm that failed to capture all the desired structure of the ideal field. The same descriptors are calculated for the trial field, e.g.,  $T = f(a_T, b_T, c_T, \dots)$ . An objective function,  $O$ , is then computed as the difference or squared difference between the ideal and trial field descriptors, e.g.,  $O = f(|a_I - a_T|, |b_I - b_T|, |c_I - c_T|, \dots)$ . The components of the objective function can be weighted to assign equal importance to small and large values or components with different units of measurement, e.g.  $O = f(w_a|a_I - a_T|, w_b|b_I - b_T|, w_c|c_I - c_T|, \dots)$ . The trial field is then perturbed, usually by replacing the value of one of the field elements with another drawn from the underlying global histogram or by swapping two nodes at random. The objective function is recalculated. Perturbations that reduce the value of the objective function are kept. Perturbations that increase the value of the objective function are accepted with a probability that decreases in proportion to the increase in objective function scaled by a parameter called the "temperature". If after each perturbation the value of  $O$  is normalized by the original value, then the formal probability rule for acceptance is a Boltzmann distribution of the form

$$P_{\text{accept}} = \exp\left(\frac{O_{\text{old}} - O_{\text{new}}}{T}\right) \quad (2)$$

where  $P_{\text{accept}}$  is the probability of accepting a perturbation,  $O_{\text{old}}$  is the normalized value of the objective function calculated before the perturbation,  $O_{\text{new}}$  is the normalized value of the objective value calculated after the perturbation, and  $T$  is the temperature, initially set to 1 (Jensen et al. 1997).

If a pre-chosen number of perturbations are accepted (usually of the order of  $10N$ , where  $N$  is the number of elements in a field) before some maximum number of total perturbations (of the order  $100N$ ), the temperature is reduced by some factor less than 1 (usually 0.1). Fast updating schemes are used to avoid completely recalculating  $O$  after every perturbation, for instance only subtracting the contribution of the perturbed field values from  $O$  and then adding the contribution of the new values (Deutsch and Journel 1992). This procedure is repeated until the objective function falls below a preselected threshold or its value can no longer be reduced. A value of  $O$  of the order  $1 \times 10^{-6}$  means that the annealed field closely matches the desired attributes encoded in the objective function.

The change in the value of  $O$  with perturbations is called the objective function trajectory. The standard implementation of annealing using Equation 2 tolerates small relative increases in the value of  $O$  while seeking to reduce its value. This feature, called "hill-climbing", allows for escape from undesirable local minima along the objective function trajectory. Steepest-descent or iterative improvement variants, where only improvements are accepted, can also be used. These variants are much faster but are prone to becoming trapped in local minima.

### Formulation of the Objective Function for Constructing Markov Fields

A Markov transition matrix can be easily encoded in an annealing objective function as a series of multipoint histograms as first described by Farmer (1992) and used by Deutsch and Journel (1992). Two-point histograms denote the expected number of transitions from any state  $i$  to any state  $j$  for a given lag in a given direction. For the forward direction of a simple Markov chain, the expected number of transitions  $f_{ij}$  between states

$i$  and  $j$  in a field of size  $n_x \cdot n_y \cdot n_z$  that uses edge wrapping to avoid edge effects (Deutsch and Cockerham 1994) is

$$f_{ij} = P(i) \cdot P(j|i) \cdot n_x \cdot n_y \cdot n_z \quad (3)$$

where  $P(i)$  is the proportion of state  $i$  and  $P(j|i)$  is the probability of transition to state  $j$  given that the chain or field is in state  $i$ . The proportion of state  $i$  is either known a priori or can be estimated by powering the transition matrix until the columns values stabilize.

In our implementation, the following objective function is enforced to generate two-dimensional, first-order fields:

$$O = \frac{1}{O^o} \left\{ \sum_{\text{idir}=1}^2 \sum_{\text{istate}=1}^{im} \sum_{\text{jstate}=1}^{im} \left( \frac{[f_{\text{idir},i,j}^{\text{train}} - f_{\text{idir},i,j}^{\text{real}}]^2}{f_{\text{idir},i,j}^{\text{train}}} \right) \right\} \quad (4)$$

where  $O$  is the value of the normalized objective function,  $i$  and  $j$  are state indices,  $im$  is the number of states,  $f_{\text{idir},i,j}^{\text{train}}$  is the number of transitions from  $i$  to  $j$  in the direction of the ideal or training image, and  $f_{\text{idir},i,j}^{\text{real}}$  is that value calculate d for the current image being annealed. The calculated value of the objective function,  $O$ , is normalized by the initial non-normalized value of  $O$ ,  $O^o$ . The squared difference between  $f_{\text{idir},i,j}^{\text{real}}$  and  $f_{\text{idir},i,j}^{\text{train}}$  is divided by  $f_{\text{idir},i,j}^{\text{train}}$  to give greater weighting to small values of transition frequencies (Deutsch and Journel 1992). We found this weighting to be necessary to satisfactorily capture between-category transition structures when annealing diagonally dominant transition matrices.

In generating the Markov structure, only the transitions from the original transition probability matrix corresponding to a lag or step size of one unit are enforced. Higher lags corresponding to higher powers of the transition probability matrix could be enforced, but our experimental observations suggested this is unnecessary to capture the first-order Markov structures. Empirically derived multipoint histograms, on the other hand, require the transitions for all lags to be enforced in order to replicate desired geometrical structures (e.g., Gooverts 1996). It should be remembered however, that any geostatistical construct can capture only some of the complexity of a natural geologic material. Other length-scale information in addition to a first-order Markov structure may be needed to adequately capture structure at longer lags. The superior utility of first-order Markov structures arises in circumstances where information pertaining to structure at long lags is lacking (Rosen and Gustofsen 1996).

### PERFORMANCE ISSUES

The main appeals to continued research in the applications of simulated annealing are: (1) its lack of an underlying statistical model, (2) its ability to condition stochastic fields with information from disparate sources, and (3) the hope that future improvement in computer performance will eventually reduce the computational expense to levels comparable to presently faster algorithms. If Markov structures are to be enforced in stochastic fields through simulated annealing, then the following performance issues need to be considered:

- Scale effects
- Complexity effects
- Implementation strategy
- Stopping criteria
- Effect of conditioning.

The impacts of these issues are illustrated by examples in this section using both synthetic and field-data-derived Markov structures.

Table 2 shows four synthetic, three-state, first-order Markov transition matrices. Each state is a color:  $B$  for black,  $G$  for gray,  $W$  for white. In the transition probability matrices 2A and 2B, all the values along the diagonal are identical, meaning that there are no differences in the average length of the bodies of each state by Equation 1. In Tables 2C and 2D, the values along the diagonals are different, implying that the average lengths are different between the three states.

TABLE 2.—Four synthetic, first-order, three-state Markov transition probability matrices and their embedded forms used in annealing experiments in this paper.

P(J) I	B	G	W	P(J) I	B	G	W
<b>B</b>	0.60	0.20	0.20	<b>B</b>	0.00	0.50	0.50
<b>G</b>	0.20	0.60	0.20	<b>G</b>	0.50	0.00	0.50
<b>W</b>	0.20	0.20	0.60	<b>W</b>	0.50	0.50	0.00
Full Transitional Matrix				Embedded Matrix			
A. 3 states, all same length scale, no embedded structure							
P(J) I	B	G	W	P(J) I	B	G	W
<b>B</b>	0.60	0.30	0.10	<b>B</b>	0.00	0.75	0.25
<b>G</b>	0.10	0.60	0.30	<b>G</b>	0.25	0.00	0.75
<b>W</b>	0.30	0.10	0.60	<b>W</b>	0.75	0.25	0.00
Full Transitional Matrix				Embedded Matrix			
B. 3 states, all same length scale, embedded structure with preferred cyclicity of B-G-W-B-G-W...							
P(J) I	B	G	W	P(J) I	B	G	W
<b>B</b>	0.60	0.30	0.10	<b>B</b>	0.00	0.75	0.25
<b>G</b>	0.075	0.70	0.225	<b>G</b>	0.25	0.00	0.75
<b>W</b>	0.15	0.05	0.80	<b>W</b>	0.75	0.25	0.00
Full Transition Matrix				Embedded Matrix			
C. 3 states with different length scales but same embedded structure as B.							
P(J) I	B	G	W	P(J) I	B	G	W
<b>B</b>	0.60	0.30	0.10	<b>B</b>	0.00	0.75	0.25
<b>G</b>	0.10	0.70	0.20	<b>G</b>	0.67	0.00	0.33
<b>W</b>	0.10	0.10	0.80	<b>W</b>	0.50	0.50	0.00
Full Transition Matrix				Embedded Matrix			
D. 3 states with same length scales as C but more complicated embedded structure.							

In the embedded form of Table 2A, there are no preferred transitions between states. In the embedded form of Table 2B, there is a preferred pattern of state-to-state transitions: B-G-W . . . , because there is three times the probability of going to state G from B than to W from B and so on. This repetition is referred to as cyclicity.

If there is asymmetry in the cyclicity if the chain direction was to be reversed, the Markov chain is said to have the property of directionality. The chain in Table 2B also shows directionality. The preferred order of the chain backwards is B-W-G rather than B-G-W. The embedded form of matrix 2C is the same as 2B. The embedded form of 2D has more of a random component because there is no preferred transition from state W to either B or G.

**Effect of Length Scale**

Annealing fields with Markov properties on finite grids becomes increasingly difficult as the length scale of the bodies become large relative to the size of the grid. Figure 2 shows the objective function trajectories for annealing single realizations of three-state, first-order structures with no embedded structure. The trajectory A corresponds to the transition probability matrix in Table 2A where the diagonal elements are 0.60. The transition probability structure was imposed isotropically in both the x and y directions on a regular 100 × 100 unit field. The other trajectories in Figure 2 represent the same matrix but where the diagonal elements have been increased to 0.70, 0.80, and 0.90. The mean categorical body lengths in the x and y directions are increasing relative to the dimension of the field (Equation 1). As the mean body length increases relative to the field size, more perturbations are required to reduce the normalized objective function to an acceptable minimum value (in this case 1 × 10<sup>-6</sup>) because the degrees of freedom available to the annealing become reduced. That is, there become increasingly fewer geometrical arrangements that satisfy O and these become harder to find by random perturbations during annealing. In the last case, where p<sub>ii</sub> = 0.90, the ratio of characteristic grid dimension (100 units) to mean body length (m<sub>ii</sub> = 9 units) is about 11 and the maximum number of perturbations at one temperature is exceeded before the stopping criterion is reached. Figure 2 also demonstrates the remedy to this

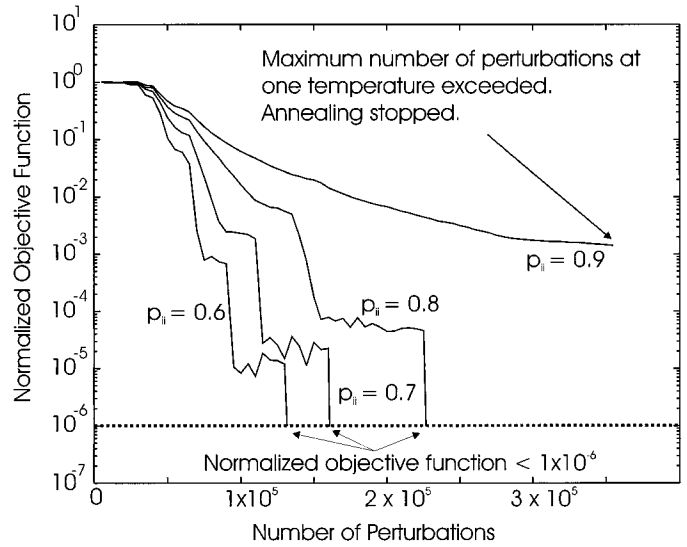


FIG. 2.—Objective function trajectories for four three-state Markov structures with no embedded structures and different categorical length scales. In 2A, p<sub>ii</sub> = 0.60 for each state; in 2B, 0.70; in 2C, 0.80; in 2D, 0.90. The corresponding mean body lengths, m<sub>ii</sub> by Equation 1 are: 2A, 1.5; 2B, 2.3; 2C, 4.0; and 2D, 9.0 units. The field size is 100 × 100 units. The ratios of field size to mean body lengths are 66.7, 42.9, 25.0, and 11.1 units, respectively. As this ratio decreases, annealing performance diminishes.

effect. By increasing the grid size relative to mean body length, the available degrees of freedom increase and thus remedy convergence problems associated with length-scale effects.

**Effects of Increasing Complexity**

Annealing performance deteriorates as the Markov structure becomes increasingly complex in terms of numbers of states, the complexity in the embedded form, and difference in length-scale distributions between states. Figure 3 shows the five objective function trajectories for single, 100 × 100 unit realizations created from Table 1 and Tables 2A through 2D. Iterative improvement was used. From the discussion above, we can see that of the five structures presented, Table 2A has the least structure—bodies of identical length-scale distributions and no embedded structure. Table 2B has bodies of identical length scales but cyclicity and directionality in the embedded structure. Table 2C has different length-scale distributions plus cyclicity and directionality whereas 2D has more randomness than 2C. Table 1, the Gloucester structure, has a greater degree of randomness in its embedded form but has five states with different length-scale distributions. The combined effect of increasing complexity and increasing length scales relative to grid size increase the number of perturbations needed to successfully anneal the field. Again, if convergence problems are encountered, a remedy is to increase the size of the grid to allow for more degrees of freedom in the annealing process.

In the case of the Gloucester structure, the slope of the objective function trajectory in this experiment is too shallow to reach the desired minimum value of O within an acceptable number of perturbations. Reasonable increases in the size of the grid (up to doubling the grid dimensions) were found not to remedy the problem. Successful annealing of the Gloucester structure on a 100 × 100 unit field was accomplished by changing the implementation strategy (discussed below).

**Implementation Strategy**

As documented in the references above, there are a number of variants of annealing that can be used to create stochastic fields. To anneal our

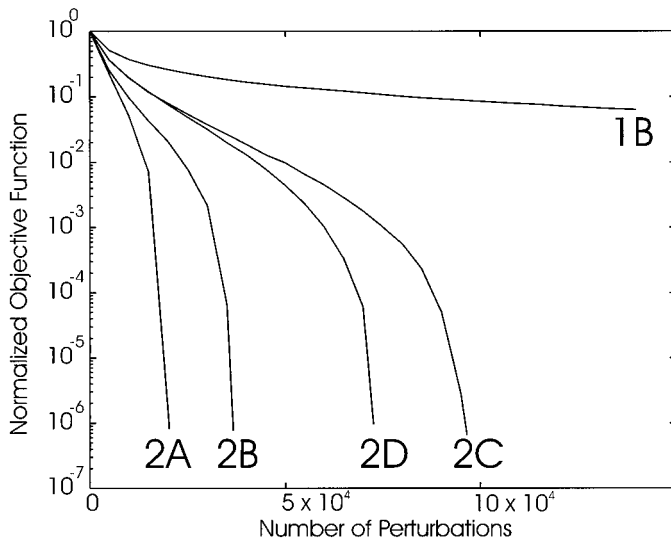


FIG. 3.—Objective function trajectories (using iterative improvement) for four three-state Markov structures (A–D) with increasingly complicated structures corresponding to those shown in Table 2A–D. The trajectory 1B is that for the five-state structure for the Gloucester clay unit in Table 1. All trajectories come from a single annealing run. Comparison of the trajectories shows that, in general, as complexity of Markov structure increases, the angle of descent of the annealing trajectory tends to decrease.

Markov fields, we used a strategy whereby the random fields were seeded with the expected proportions of each state determined by powering the transition probability matrix until the column values stabilized. Perturbations were done by swapping pairs of grid values selected at random. In general, iterative improvement performed acceptably well with three-state, first-order Markov structures. As length scales, number of states, complicated embedded structures, etc. were incorporated, true annealing with “hill-climbing” tends to perform better.

In the case generating a  $100 \times 100$  unit field for the five-state Gloucester transition structure, neither true annealing or iterative improvement were sufficient on their own to reduce the normalized objective function below an acceptable threshold,  $O < 10^{-5}$ , in an acceptable number of perturbations. The objective function trajectories for two attempts are shown in Figure 4. In the case of using iterative improvement alone (Trajectory A), the objective function trajectory in this single attempt became trapped in an unacceptable local minimum. Note that changing the initial random number seed may improve performance between realizations, but the goal of efficient implementation in this case is to successfully anneal each realization attempted, not a random subset.

In the case of pure annealing alone, the objective function trajectory did not descend quickly enough to reach the desired threshold in less than  $2 \times 10^7$  perturbations (first segment of Trajectory B). Slowing or accelerating the cooling schedule by the using a 0.9 or 0.01 multiplier (instead of 0.1) on  $T$  after each time  $10 \cdot N$  acceptable perturbations were accepted did not improve annealing performance in this case. However, post-processing the outcome of true annealing with iterative improvement was found to produce satisfactory results (second segment of Trajectory B).

**Stopping Criterion**

In most applications of annealing, a very small value of normalized objective function is used as the stopping criterion or rule. The choice of how small is small enough is found through experiment. Very small values may not be achievable in cases where multi-part objective functions are used. Use of a very low value implies a high degree of confidence in the value of the idealized or training measures embedded in the objective func-

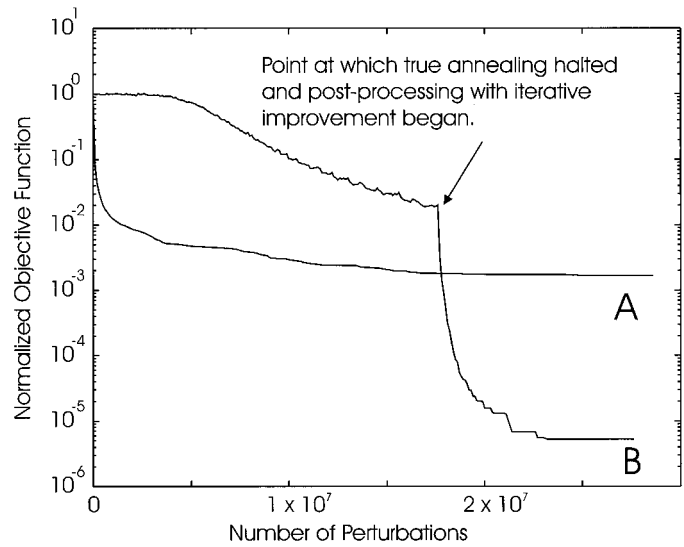


FIG. 4.—Objective function trajectories for the five-state Markov structure in Table 1 comparing the annealing performance of iterative improvement (Trajectory A) to that of true annealing post-processed with iterative improvement (Trajectory B). The combined approach succeeded in reducing the objective function value to an acceptable minimum whereas the iterative improvement approach became trapped in an unacceptable minimum. The performance of true annealing alone (first segment of Trajectory B) also was unsuccessful in reducing the objective function to an acceptable minimum within a tolerable number of perturbations.

tion. But in earth science applications, our information from the subsurface and even outcrop is often incomplete. Matching the Markov transition frequencies exactly may not be warranted.

As mentioned in the introduction, a chi-squared test statistic can be used determine if an observed Markov chain or its embedded form are significantly different from a random series of events. The same formulation can be used to determine if two Markov transition matrices are different from each other at some level of statistical significance (Powers and Easterling 1982). Table 3 compares the values of the normalized objective function and associated numbers of perturbations needed to anneal a single isotropic field with the structure of Table 2C with different stopping criteria based on the chi-squared test statistic. One can see that, as the level of statistical significance used in the chi-squared test decreases from 0.20 to 0.01, it becomes increasingly easy to accept that the annealed field is not significantly different from the training structure with commensurate computational savings in the form of fewer perturbations. Figure 5 shows the same stopping points on a plot of the objective function trajectory. Because iterative improvement was used in this relatively simple example, the objective function trajectory is quite steep and the computational savings associated with using a chi-squared test as a stopping criterion are not pro-

TABLE 3.—A comparison of final normalized objective-function values and number of perturbations associated with using a conventional annealing stopping criterion and using a chi-squared test statistic for similarity between the trial image and the training structure. The trial image was a  $100 \times 100$  unit field with the first-order Markov structure in Table 1C. Results are shown graphically in Figure 5.

Stopping Criteria	Normalized Objective Function	Number of Perturbations
Objective Function $< 1e-6$ ( $\chi^2_{crit} = 0.641e-01$ )	0.650e-06	96589
$\chi^2_{crit} < \chi^2_{\alpha, \nu} = 5.99: \alpha = 0.20, \nu = 4$	0.830e-04	88663
$\chi^2_{crit} < \chi^2_{\alpha, \nu} = 7.78: \alpha = 0.10, \nu = 4$	0.108e-03	87639
$\chi^2_{crit} < \chi^2_{\alpha, \nu} = 9.49: \alpha = 0.05, \nu = 4$	0.132e-03	86809
$\chi^2_{crit} < \chi^2_{\alpha, \nu} = 11.14: \alpha = 0.025, \nu = 4$	0.154e-03	86233
$\chi^2_{crit} < \chi^2_{\alpha, \nu} = 13.28: \alpha = 0.01, \nu = 4$	0.188e-03	85455

$\alpha$  = level of significance  $\nu$  = degrees of freedom.

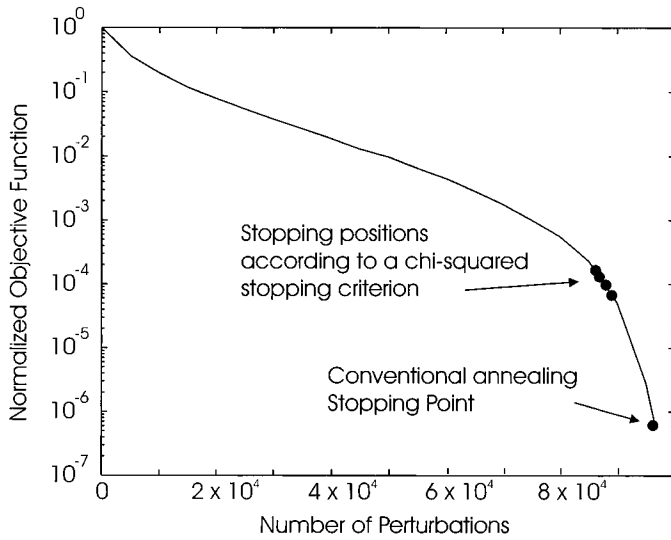


FIG. 5.—Stopping points from Table 3 placed on the objective function trajectory (iterative improvement used).

found. However, when the objective function becomes less steep, the computational savings associated with reaching a normalized objective function value on the order of  $1 \times 10^{-3}$  or  $1 \times 10^{-4}$  can be substantial compared to the effort needed to reach a more conventional stopping criterion like  $O < 1 \times 10^{-6}$ .

TABLE 4.—A synthetic, second-order, three-state Markov structure (A, B, and C) with the associated or embedded first-order Markov structure (D) for comparison. These structures are used to create the images in Figure 7.

	B	G	W		B	G	W	
B	0.85	0.075	0.075	A. $P(K) J I = B$	B	0.65	0.175	0.175
G	0.075	0.85	0.075		G	0.20	0.55	0.25
W	0.075	0.075	0.85		W	0.20	0.55	0.25
								B. $P(K) J I = G$
	B	G	W		B	G	W	
B	0.60	0.20	0.20	C. $P(K) J I = W$	B	0.80	0.10	0.10
G	0.35	0.25	0.40		G	0.21	0.50	0.29
W	0.25	0.25	0.50		W	0.23	0.25	0.52
								D. $P(K) J$

Effects of Conditioning

Stochastic images generated by annealing can be constrained or “conditioned” to honor field observations simply by assigning the appropriate grid locations the observed values and not perturbing them. This approach produces undesirable discontinuities in the vicinity of the conditioning data (Deutsch and Journel 1992). The discontinuities can be smoothed by weighting the contribution of any part of the global objective function involving conditioning data heavier than nonconditioning grid blocks (Deutsch and Cockerham 1994). However, adding weights to conditioning nodes reduces the degrees of freedom and makes it more difficult to lower the value of  $O$  by annealing. Figure 6 shows an experiment wherein a  $100 \times 100$  unit field with the structure in Table 2C was conditioned to match data from a vertical “well” of lengths 5, 25, and 100 units. The values of the well data were obtained by sampling a different unconditional reali-

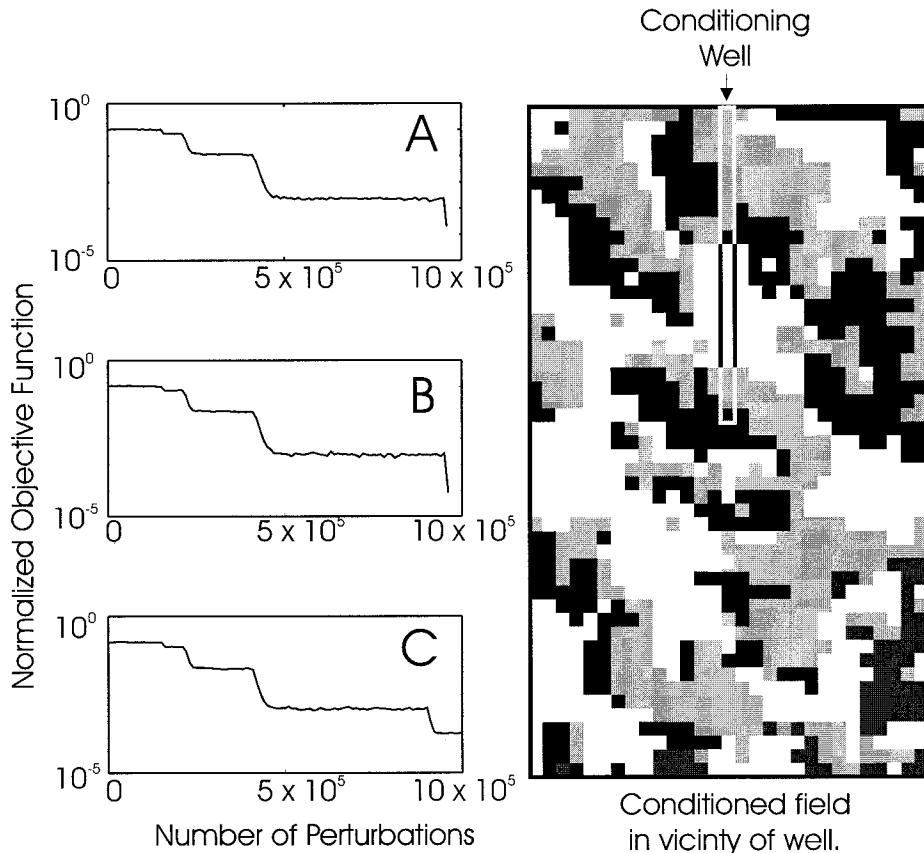


FIG. 6.—Effect of conditioning on annealing performance. Trajectories on left show annealing performance when a  $100 \times 100$  unit, three-state field is conditioned to honor a vertical well of length A: 5 units, B: 25 units, and C: 100 units. True annealing was used. Stopping criterion is when the calculated chi-squared test statistic fell below 13.2, corresponding to a level of significance of 0.01 and 4 degrees of freedom. Run C became trapped in a local minimum before satisfying the stopping criterion. The weighting on the conditioning pairs was set to 5.0. The field on the right shows detail of field B in the vicinity of the conditioning well (outline). The underlying Markov structure is that in Table 2C.

zation with the same structure. In this case, a weighting of 5 was used on transition probabilities that involved conditioning data. For the cases of wells of lengths 5 and 25 units, true annealing reached a satisfactory threshold of the normalized objective function based on a chi-squared test statistic at a 0.01 level of significance. The detail of the well around the 25-unit well shows that the field has been acceptably smoothed. We found that weights higher than 5 degraded the annealing performance rapidly. For example, the objective function trajectory for the field conditioned by a 100-unit well in Figure 6C became trapped in an unacceptable local minimum before passing the chi-squared threshold. Using a weighted formulation of the objective function to condition an annealed field to field data has the effect of reducing the number of degrees of freedom. Because the weights are found by trial and error, if increased weights are necessary to achieve a desired degree of local smoothing around data points but result in degraded annealing performance, extending the grid is the first remedy that should be considered because it increases the available degrees of freedom.

#### CAPTURING GEOLOGICALLY MEANINGFUL STRUCTURES IN STOCHASTIC FIELDS WITH MARKOV STRUCTURES

The previous section demonstrated that imbuing stochastic fields with Markov properties is reasonably straightforward using simulated annealing provided that attention is paid to some key performance issues. In this section we look at some examples of styles of stratal architecture that can be embedded in stochastic fields by this approach. The first examples shown are synthetic but they demonstrate some of the potential of applying this technique to simulation of real rock systems. In the final example, an unconditioned stochastic image of the Gloucester clay unit is presented to demonstrate that these ideas can be carried out with field data.

##### Example 1: First-Order versus Second-Order Structure

Markov chains and fields can possess a higher than single order structure. Higher-order structures are discussed in detail in Harbaugh and Bonham-Carter (1970), although convincing examples of Markov structures of second or higher order are uncommon in the geological literature. Harbaugh and Bonham-Carter (1970) suggested that double dependency in bedding sequences may be the signature of two independent forcings on a depositional system that act on different time scales. For example, one might look for higher-order Markov structure when a low-frequency depositional process is superimposed on a higher-frequency process, like relative sea-level variation affecting Markov transitions at long lags while autocyclic depositional processes like delta-lobe switching control transition probabilities over short lags.

Table 4 shows a synthetic, three-state structure. The second-order structure is shown in the form of three transition probability matrices. Matrix 4A shows the transition probability structure associated with going from State  $J$  at location  $\mathbf{x}$  to State  $K$  at  $\mathbf{x} + 1$  given that the Markov chain is in state  $I = \text{Black}$  at the prior location  $\mathbf{x} - \tau$ , where we have arbitrarily chosen  $\tau = 9$  grid units. Likewise, Matrix 4B shows transition probabilities associated with going from  $\mathbf{x}$  to  $\mathbf{x} + 1$  if the Markov chain is in state "Gray" at  $\mathbf{x} - 9$  and 4C shows the probabilities if the Markov chain is in state "White" at  $\mathbf{x} - 9$ . Table 4D shows the first-order Markov structure embedded in the second-order structure of Table 4A–C. Two  $100 \times 100$  unit fields were generated by annealing using multipoint histograms to enforce the second-order structure as well as the first-order structure of Table 4.

These two fields are shown as gray-scale images in Figure 7. From the gray-scale images, it appears that the second-order Markov image has a different structure than the first-order image. Indicator variograms for each state are also shown in Figure 7. Indicator variograms are nondirectional geostatistical constructs that capture the structure in categorical fields (see Carle and Fogg 1996 for a complete discussion of indicator geostatistics

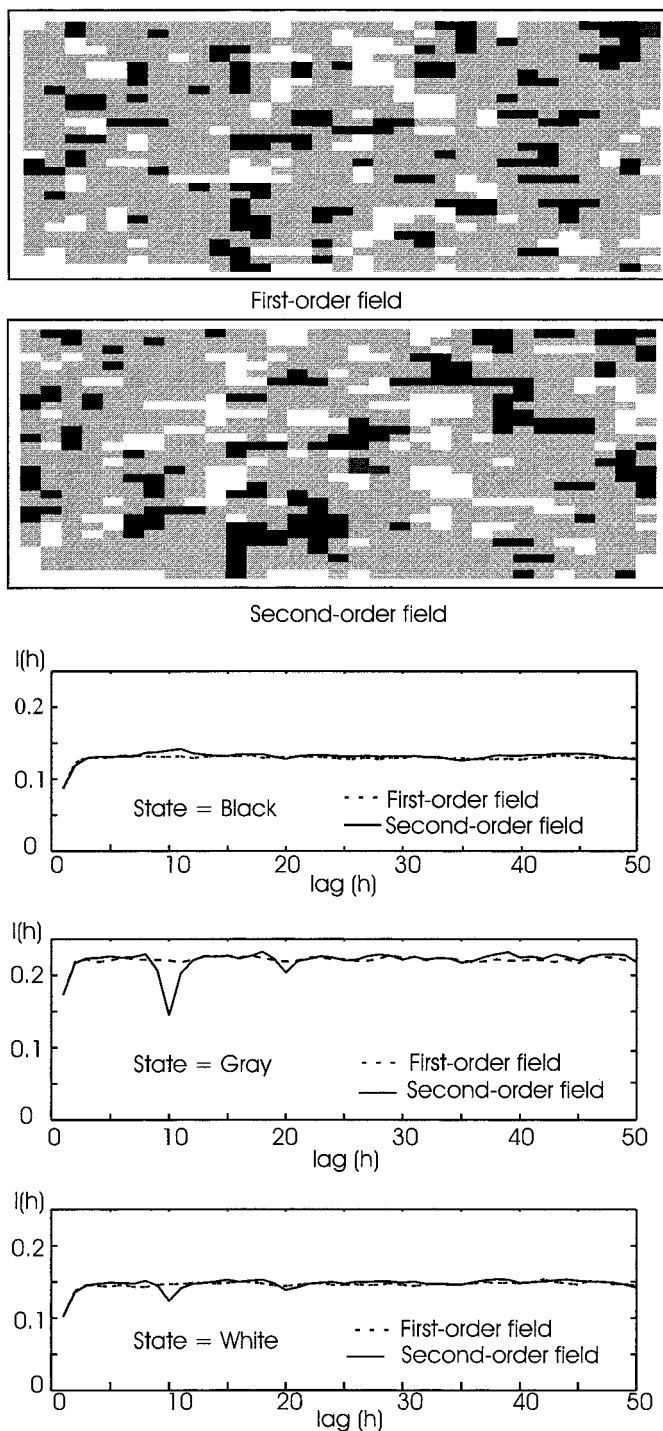


FIG. 7.—Comparison of first-order and second-order, three-state Markov fields as shown in Table 4. Comparative indicator variograms are shown for each state. The gray and white states show a strong reduction in indicator semivariance at the lag corresponding to the spatial wavelength of the second-order structure.

in a Markov context). The gray and white categories show strong reduction in indicator variogram values lags corresponding to the spatial wavelength of the second-order structure. These variogram structures are capturing a measure of the additional statistical structure in the second-order Markov image that is lacking in the first-order Markov image.

TABLE 5.—A synthetic, first-order, three-state Markov structure showing both directionality and cyclicity (A) and the same structure after directionality and cyclicity has been removed by averaging off-diagonal elements (B). Comparison of accompanying eigenvalues shows that A has the complex eigenvalues diagnostic of cyclicity whereas B does not. These structures are used to create the images in Figure 8.

P(J) I	B	G	W	P(J) I	B	G	W
<b>B</b>	0.60	0.37	0.03	<b>B</b>	0.60	0.20	0.20
<b>G</b>	0.03	0.60	0.37	<b>G</b>	0.20	0.60	0.20
<b>W</b>	0.37	0.03	0.60	<b>W</b>	0.20	0.20	0.60

Eigenvalues:		Eigenvalues:	
	1.00		1.00
	0.4 + .294i		0.40
	0.4 - .294i		0.40

A B

**Example 2: Directionality and Cyclicity**

The concepts of directionality and cyclicity in Markov Chains were introduced above. Directionality is common in many sedimentary depositional environments, e.g., consider shoaling-upward sequences on carbonate banks or fining-upward sequences in channel deposits. Directionality means that there is an up-and-down or a basinward and landward asymmetry in a bedding sequence. Cyclicity or the regular, nonrandom repetition of beds is also common in the rock record. In Markov chains, cyclicity is detected by the presence of complex eigenvalues in the transition probability matrix (Schwarzacher 1975). The synthetic transition probability matrix in Table 5A has obvious cyclicity and has complex eigenvalues as shown. Directionality is also evident in the embedded form—there is a distinct directionality in the off-diagonal elements that would change if the chain is run backwards. A single two-dimensional field with this transition matrix en-

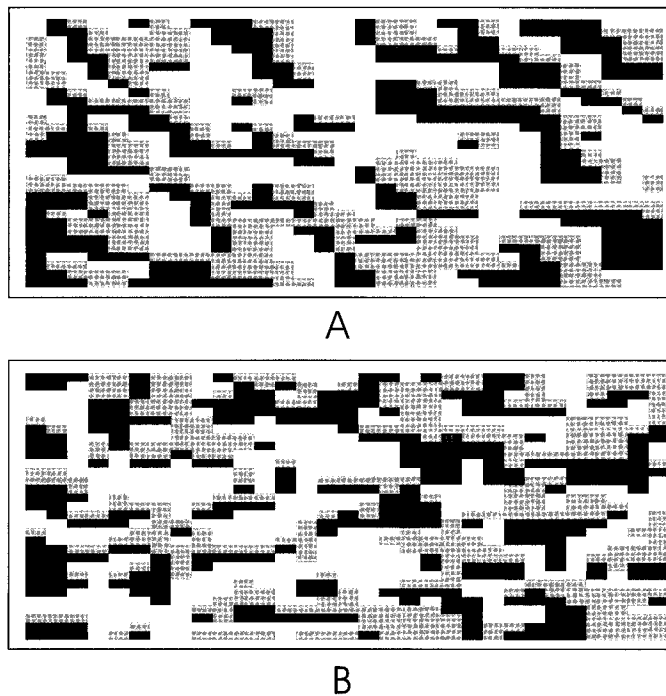
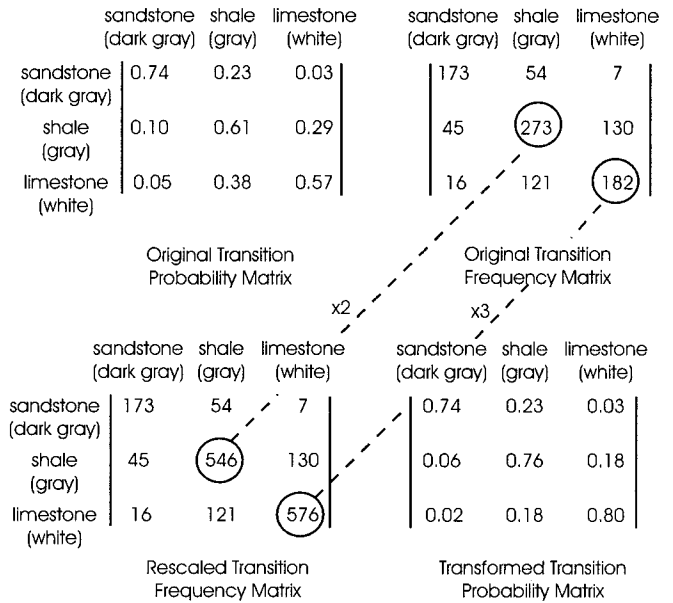
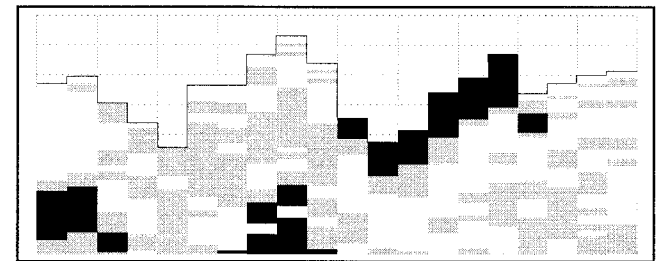


FIG. 8.—Comparison of detail from two 100 × 100 unit fields honoring the first-order, three-state Markov structures in Table 5. In field A, the directionality and cyclicity of Table 5A is enforced in both the vertical and the horizontal. Field B is a hybrid field, combining the structure of Table 5A in the vertical and that of 5B (no directionality or cyclicity) in the horizontal.



A



B

FIG. 9.—Illustration of conversion of a three-state Markov field from spatial coordinates to equivalent temporal coordinates and back using relative rates of deposition to rescale vertical categorical length scales. Field A is generated in mixed time-space coordinates with time in the vertical. Field B is the same but back-transformed to pure spatial coordinates.

forced in the vertical and horizontal directions is shown as a grayscale image in Figure 8A. Note the preferred transitions going black–gray–white–black in the upward and rightward directions.

For comparison, the directionality and cyclicity was removed in the horizontal direction by averaging the off-diagonal elements in the Markov structure as shown in Table 5B. Note that the complex eigenvalues have now disappeared. The symmetric structure of Table 5B was enforced in the horizontal in the grayscale image in Figure 8B, leaving the vertical structure as before in Table 5A, i.e., two different transition matrices are being enforced in orthogonal directions. The preferred pattern of black–

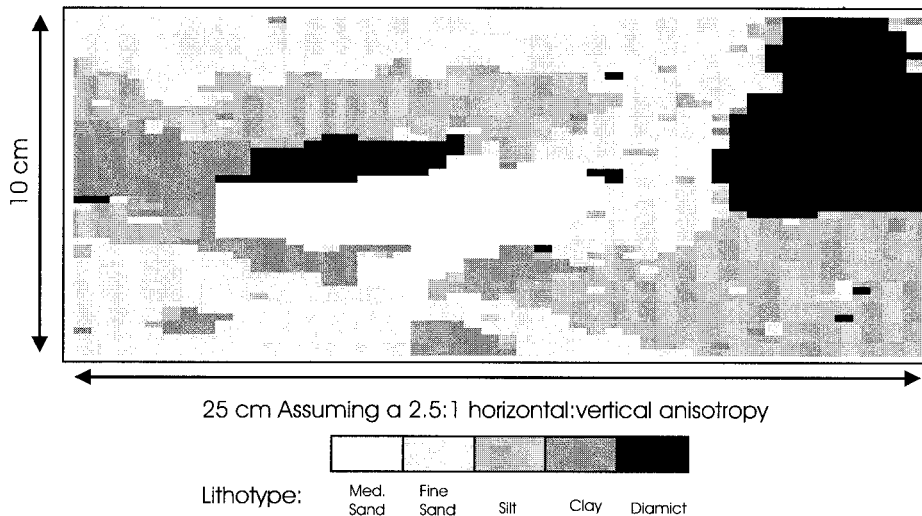


FIG. 10.—Unconditional panel reproduction of the Gloucester clay unit generated shown in Table 1. The field was generated by the combined approach shown in Figure 4.

gray–white–black transitions persists in the upward vertical but in the horizontal rightward direction has disappeared.

This example highlights the flexibility of annealing to capture hybrid structures that better accommodate geological concepts of reasonableness. There are many geological environments where directionality and cyclicity are apparent in vertical bedding relationships but do not extend to relationships in the horizontal.

### Example 3: Honoring Time-Spatial Relationships in Markov Representations of Strata

If Walther's Law of facies succession is used to justify transfer of Markov measures of vertical variability in bedding sequences to the horizontal, a coordinate transformation from vertical space to vertical time must be considered to ensure that horizontal surfaces equal time lines. The coordinate transformation necessary to transfer vertical Markov measures to the horizontal along time lines is a simple rescaling of each category separately according to their relative depositional rates. The mechanics of this rescaling (Schwarzacher 1969) is shown in Figure 9A, where a synthetic sandstone–shale–limestone system is rescaled from transitions counted in space to equivalent transitions in time assuming that the relative depositional rates of sandstone, shale, and limestone are 1.0, 0.5, and 0.33, respectively. This rescaled Markov temporal structure was enforced in the vertical direction of a  $100 \times 100$  field in Figure 9B whereas the horizontal structure enforced was the original Markov spatial structure. This realization was back-transformed to vertical spatial coordinates by post-processing in such a way as to compress the limestone and shale pixels vertically in inverse proportion to their relative rates of deposition. Markov fields constructed in a Waltherian framework should conserve the sediment, time, and volume elements of a depositional system. Prior to vertical back-transformation, such Markov fields could be regarded as synthetic Wheeler diagrams (Wheeler 1958).

If desired, compaction effects can be similarly incorporated. Similarly, significant gaps in the sedimentary record due to erosion and nondeposition are accounted for as a nondepositional or erosional state existing through time. It is conceivable that if sufficient geochronological or biostratigraphic data exist to reconstruct these states, they could enter a Markov model as a category in a mixed vertical time-horizontal space coordinate system that is subsequently removed in the back-transformation to vertical space coordinates.

### Example 4: A Stochastic Image of the Clay Unit at the Gloucester Site

Figure 10 shows the final example: a  $100 \times 100$  2D stochastic image representing part of the 3 m clay unit at the Gloucester site. All of the

structure encapsulated in the Markov transition matrix in Table 1 is present in this image. The effort required to anneal this image was shown above in Figure 4. Annealing this image was difficult, but not impossible, because of the number of states present, the low ratio of grid size to mean body lengths, and the complexity of the structure. Unfortunately there are no outcrops to validate this particular stochastic reconstruction. However, this example demonstrates that field data can be gathered from borehole cores, translated into a meaningful Markov probability structure and used to inform a stochastic image of a complex geological system by annealing. Such a categorical field could be further populated with fine-scale grid values of porosity and permeability to render the image suitable for use in flow simulation.

### SUMMARY

In this paper, we demonstrate how conditioned structured fields honoring Markov transition probability structures can be generated with simulated annealing. To guide future applications of this technique, performance issues pertaining to scale effects, structural complexities, and choice of stopping criteria were discussed and remedies offered, namely:

*Scale Effects.* As categorical length scales increase relative to grid size, annealing performance diminishes. The general remedy is to use a larger grid.

*Complexity Effects.* As number of states, variation in categorical length scales, or complexity in the embedded Markov chain increase, annealing performance diminishes. The remedy is to choose a larger grid or possibly try a combination of annealing routines.

*Stopping Criteria.* To remedy complexity effects or to reduce computational cost, a chi-squared test statistic can be used to evaluate if the annealed image is significantly different than the training image at some predetermined level of confidence. This approach can be justified when the Markov model is being estimated from incomplete subsurface data or is otherwise incompletely known. Incorporation of such a stopping criterion can be also considered when Markov structures are to be blended with other kinds of structures in an objective function.

By incorporating Markov structures in stochastic simulation of real rock systems, one can capture more geologic realism. We show how Markov structures can capture geological complexities in natural systems pertaining not only to length scales and interrelationships between categories but also stratal architecture reflecting aspects of depositional process: higher-order structures, cyclicity, and directionality. The flexibility of this approach to accommodate geological reasoning through hybrid structures and rescaling to honor time-space relationships in real rock systems was highlighted. An

example is shown where field data taken from borehole cores were successfully transmitted to a stochastic image by this method.

#### ACKNOWLEDGMENTS

This work has been supported through the Amoco Canada Petroleum Company Ltd. Graduate Fellowship in Geology at the University of Calgary. Additional support has been provided by the Environment Canada through the National Water Research Institute of the Canada Centre for Inland Waters, the Canada National Science and Engineering Research Council Grant No. OGP0122023, and the Department of Geology and Geophysics, University of Calgary. This manuscript benefited from the thoughtful reviews of David Mohrig, Anil Deshpande, and an anonymous reviewer for the Journal.

#### REFERENCES

- CARLE, S.F., AND FOGG, G.E., 1996, Transition probability-based indicator geostatistics: *Mathematical Geology*, v. 28, p. 453–478.
- CHEN, Q., 1999, Markov processes and discrete multifractals: *Mathematical Geology*, v. 31, p. 455–470.
- DAVIS, J.C., 1986, *Statistics and Data Analysis in Geology*: New York, Wiley, 646 p.
- DEUTSCH, C.V., AND COCKERHAM, P.W., 1994, Practical considerations in the application of simulated annealing to stochastic simulation: *Mathematical Geology*, v. 26, p. 67–82.
- DEUTSCH, C.V., AND HEWITT, T.A., 1996, Challenges in reservoir forecasting: *Mathematical Geology*, v. 28, p. 829–842.
- DEUTSCH, C.V., AND JOURNEL, A.G., 1992, *GSLIB Geostatistical Software Library and User's Guide*: New York, Oxford University Press, 340 p.
- DOVETON, J.H., 1994, Theory and Application of Vertical Variability Measures from Markov Chain Analysis, in Yarus, J.M., and Chambers, R.L., eds., *Stochastic Modeling and Geostatistics—Principles, Methods and Case Studies*: American Association of Petroleum Geologists, *Computer Methods in Geology* 3, p. 55–64.
- FARMER, C.L., 1992, Numerical Rocks, in King, P.R., ed., *Proceedings of the First European Conference on the Mathematics of Oil Recovery*: New York, Oxford University Press, p. 437–448.
- FULTON, R.J., ANDERSON, T.W., GADD, N.R., HARINGTON, C.R., KETTLES, I.M., RICHARD, S.H., RODRIGUES, C.G., RUST, B.R., AND SHILTS, W.W., 1987, Summary of the Quaternary of the Ottawa Region, in Fulton, R.J., ed., *Quaternary of the Ottawa Region and Guides for Day Excursions*: International Union for Quaternary Research, XXII Congress, July 31–August 8, 1987, p. 7–22.
- GOOVERTS, P., 1996, Stochastic simulation of categorical variables using a classification algorithm and simulated annealing: *Mathematical Geology*, v. 28, p. 909–921.
- HARBAUGH, J.W., AND BONHAM-CARTER, G., 1970, *Computer Simulation in Geology*: New York, Wiley, 575 p.
- JACKSON, R.E., LESAGE, S., PRIDDLE, M.W., CROWE, A.S., AND SHIKAZE, S., 1991, Contaminant Hydrogeology of Toxic Organic Chemicals at a Disposal Site, Gloucester, Ontario. 2. Remedial Investigation: Inland Waters Directorate Scientific Series No. 181, Burlington, Ontario, National Water Research Institute, Environment Canada, 68 p.
- JENSEN, J.L., LAKE, L.W., CORBETT, P.W.M., AND GOGGIN, D.J., 1997, *Statistics for Petroleum Engineers and Geoscientists*: Englewood Cliffs, New Jersey, Prentice Hall, 390 p.
- KOLTERMANN, C.E., AND GORELICK, S.M., 1996, Heterogeneity in sedimentary deposits: A review of structure-imitating, process-imitating, and descriptive approaches: *Water Resources Research*, v. 32, p. 2617–2658.
- KRUMBEIN, W.C., 1967, Fortran IV Computer Programs for Markov Chain Experiments in Geology: Kansas State Geological Survey, Computer Contribution 13.
- LIN, C., AND HARBAUGH, J.W., 1984, *Graphic Display of Two- and Three-Dimensional Markov Computer Models in Geology*: New York, Van Nostrand Reinhold, 180 p.
- LUO, J., 1996, Transition probability approach to statistical analysis of spatial qualitative variables in geology, in Forster, A., and Merriam, D.F., eds., *Geologic Modeling and Mapping*: New York, Plenum Press, p. 281–297.
- MIALL, A.D., 1980, Cyclicity and the facies model concept in fluvial deposits: *Bulletin of Canadian Petroleum Geology*, v. 28, p. 59–80.
- MIDDLETON, G.V., 1973, Johannes Walther's Law of the Correlation of Facies: *Geological Society of America, Bulletin*, v. 84, p. 979–988.
- MOSS, B.P., 1990, Stochastic reservoir description: a methodology, in Morton, A.C., Hurst, A., and Lovell, M.A., eds., *Geological Applications of Wireline Logs*: Geological Society of London, Special Publication 48, p. 57–76.
- MURRAY, C.J., 1994, Identification and 3-D Modeling of Petrophysical Rock Types, in Yarus, J.M., and Chambers, R.L., eds., *Stochastic Modeling and Geostatistics—Principles, Methods, and Case Studies*: American Association of Petroleum Geologists, *Computer Applications in Geology* 3, p. 55–64.
- OUENES, A., AND BHAGAVAN, S., 1994, Application of simulated annealing and other global optimization methods to reservoir description: myths and realities: Society of Petroleum Engineers, 1994 Annual Technical Conference and Exhibition, New Orleans, September 25–28 1994, SPE Paper 28415.
- POWERS, D.W., AND EASTERLING, R.G., 1982, Improved methodology for using embedded Markov chains to describe cyclical sediments: *Journal of Sedimentary Petrology*, v. 52, p. 913–923.
- RUST, B.R., 1977, Mass flow deposits in a Quaternary succession near Ottawa, Canada; diagnostic criteria for subaqueous outwash: *Canadian Journal of Earth Sciences*, v. 14, p. 175–184.
- SCHWARZACHER, W., 1969, The use of Markov chains in the study of sedimentary cycles: *Mathematical Geology*, v. 1, p. 17–39.
- SCHWARZACHER, W., 1975, *Sedimentation Models and Quantitative Stratigraphy*: New York, Elsevier, 382 p.
- WALKER, R.G., 1979, Facies and Facies Models—General Introduction, in Walker, R.G., *Facies Models*, 1st Edition: Geoscience Canada, Reprint Series 1, p. 1–8.
- WHEELER, H.A., 1958, Time stratigraphy: American Association of Petroleum Geologists, *Bulletin*, v. 42, p. 1047–1063.
- XU, H., AND MACCARTHY, A.J., 1996, Markov chain analysis of vertical facies sequences using a computer software package (SAVFS): Courtmacsherry Formation (Tournaian), Southern Ireland: *Computers & Geosciences*, v. 24, p. 131–140.

Received 9 March 1999; accepted 9 December 1999.